http://dx.doi.org/10.5012/bkcs.2013.34.7.2162

The Effect of Low-Temperature Carbon Encapsulation on Si Nanoparticles for Lithium Rechargeable Batteries

Jaepyeong Jung, Kyeongse Song, and Yong-Mook Kang*

Department of Energy and Materials Engineering, Dongguk University-Seoul, Seoul 100-715, Korea
**E-mail: dake1234@dongguk.edu*
Received March 23, 2013, Accepted April 26, 2013

The tailored surface modification of electrode materials is crucial to realize the wanted electronic and electrochemical properties. In this regard, a dexterous carbon encapsulation technique can be one of the most essential preparation methods for the electrode materials for lithium rechargeable batteries. For this purpose, DL-malic acid ($C_4H_6O_5$) was here used as the carbon source enabling an amorphous carbon layer to be formed on the surface of Si nanoparticles at enough low temperature to maintain their own physical or chemical properties. Various structural characterizations proved that the bulk structure of Si doesn't undergo any discernible change except for the evolution of C-C bond attributed to the formed carbon layer on the surface of Si. The improved electrochemical performance of the carbon-encapsulated Si compared to Si can be attributed to the enhanced electrical conductivity by the surface carbon layer as well as its role as a buffering agent to absorb the volume expansion of Si during lithiation and delithiation.

Key Words : Low-temperature carbon coating, DL-malic acid, Si, Anode, Lithium rechargeable batteries

Introduction

Increasing awareness of environmental pollution and limited energy resources led to a profound evolution in the way how we see the energy-related problems. Although fossil and nuclear sources will remain the most important energy providers for many years, the solutions for the concurrent energy problems, which involve the alternative means of energy storage need to be urgently developed. Among various technologies, lithium rechargeable batteries (LIBs) are one of the most important power sources for various existing and potential applications including popular mobile devices, next generation electric and hybrid-electric vehicles (EVs/HEVs) because of their relatively high specific energy density.[1-3]

The electrochemical performance of lithium rechargeable batteries strongly depends on the capacity, norminal voltage, cycling stability and etc. of electrode materials. Graphitic carbons have been mainly used for the anodes in commercial lithium rechargeable batteries. Because graphitic carbons have the theoretical capacity limitation below 372 $mAhg^{-1}$, considerable researches have been conducted to search out the possible alternative anode materials exhibiting higher capacity.[4-6] As a result, several alternative anode materials have been proposed for lithium rechargeable batteries, such as silicon,[7-12] tin,[13-16] and germanium[17] because they are all capable of alloying with more lithium than graphitic carbons. Particularly, Si has the highest theoretical capacity of 4200 $mAhg^{-1}$ when forming $Li_{4.4}Si$ alloys, far greater than that of graphitic carbon.[18] However, during alloying and dealloying process with Li, Si exhibits significant volume changes corresponding to approximately 400% of the original volume. This enormous volume expansion may well cause the pulverization of individual particles finally breaking down the electrically conductive network inside the electrode.[19] In order to exclude this problem, many studies have been just focusing on the reduction of particle size on the ground of previous report stressing out that the volume change inside Si lattice during alloying with Li are inversely proportional to its particle size. However, Si nanoparticles not only are vulnerable to acidic attack attributed to organic electrolytes but also inevitably undergo a drastic agglomeration for the thermodynamic reason (the decrease of surface free energy), which intensifies particle pulverization accompanied by capacity fading during cycling. In an attempt to overcome these significant drawbacks, several typical approaches have been developed to improve the lifespan of Si electrode. One way is to prevent its pulverization by constructing the invulnerable nanostructures with various morphologies such as nanowires, nanonets, nanofibers, and nanotubes or by surface modification using conductive species like silver, carbon and so on.[20-25] Great electron conductors such as carbonaceous materials and carbon nanotubes are well documented that can additionally help to enhance the electronic conduction during electrochemical reactions. The enhanced electrochemical properties of carbon composites prepared through mechanical milling, hydrothermal method, and chemical vapor deposition[28] have been also reported. However, most of the methods for these surface modifications have negatively affected the physical and/or chemical properties of electrode materials. Actually, these processes involving high energy can cause significant morphological change,[26] oxidation[27] and side reaction[28] finally evolving inactive intermetallic compound such as silicon carbide in some cases. Morphological changes sometimes alter the electrochemical reaction route of active materials[29] and the

involved reaction site limitation can induce more serious volume expansion. Furthermore, the formation of silicon carbide results in significant capacity loss due to its inactivity with Li^+. Therefore, the effective carbon coating around Si without its structural change has remained as an open problem. In this regard, here we report a relatively-low-temperature process instead of high-temperature thermal pyrolysis, to prepare a conductive carbon layer without any mechanical damage to the bulk structure of electrode materials. Furthermore, the evaluation on the electrochemical performance of our Si/C nano-composite shows significant cyclic and kinetic improvements due to carbon layer which serves as both efficient electron transport pathway and rigid mechanical support.

Experimental

Preparation of Si/Carbon Nano-Composite. Figure 1(a) schematically presents the synthesis sequence of Si/Carbon nano-composite. DL-Malic acid ($C_4H_6O_5$, 99%) was used to apply carbon coating on the surface of Si nanoparticles. Considering its low melting point (131 °C) and high solubility in an organic solvent, DL-malic acid ($C_4H_6O_5$) was chosen as the carbon source. The DL-malic acid was thoroughly dissolved in toluene. When the solution become transparent, Si nanoparticles were added into the solution and stirred homogeneously for 2 h under H_2 (5%)/Ar ambient. The ratio of DL-malic acid to Si nanoparticles was fixed at 1:1 (wt %). The mixture solution was continuously stirred for 6 h at 180 °C in vacuum condition. DL-Malic acid was heated to 265 °C under Ar and holded for 3 h after that, for carbonization as below the eqn.

$$Si + C_4H_6O_5 \rightarrow Si+3C + CO_2(g)\uparrow + 3H_2O(g)\uparrow \quad (1)$$

This reaction indicates the thermal decomposition process of DL-malic acid. As shown here, DL-malic acid decomposes into amorphous carbon through the evaporation of carbon dioxide and water. All chemicals and solvents were used without additional purification.

Electrochemical Measurements. The electrodes were fabricated by mixing each active material of Si/Carbon nano-composite, acetylene black and polyimide (PI) with a weight ratio of 8:1:1 using *N*-methylpyrrolidone (NMP) as a solvent. The resulting slurries were pasted onto Cu foils and then dried in a vacuum oven at 110 °C for 5 h. Then, the electrode was cured at 350 °C for 1 h under Ar ambient. Next, instantly the electrode was dried at 60 °C for 4 h in a vacuum oven. The electrochemical properties of the prepared electrodes were evaluated using the CR2016 coin-type cells assembled in an argon-filled glove box. Li metal foil was used as a counter electrode and the electrolyte was 1.3 M of $LiPF_6$ dissolved in a 1:1 (v/v) mixture of ethylene carbonate (EC) and diethylene carbonate (DEC) with 5% FEC additive. For the first cycle, the cells were galvanostatically charged and discharged at a current density of 210 mAg^{-1} over a range of 0.005 V to 1.5 V. Then it was cycled at 420 mAg^{-1} up to 30th cycle between 0.005 V and 1 V. To analyze the electrochemical impedance response, a Solartron 1255 frequency response analyzer (FRA) was used in conjunction with the Solartron 1286 electrochemical interface.

Characterizations. The Si nanoparticles and Si/Carbon nano-composite were identified by the X-ray diffraction (XRD; Rigaku D/Max-RB diffractometer, using Cu Kα radiation at 40 kV and 100 mA), the field emission scanning electron microscopy (FE-SEM; TESCAN MIRA LMH2, operated at 15 kV), the high resolution transmission electron microscope (HR-TEM; JEOL JEM-3010). Raman spectroscopy was conducted using a commercial apparatus (MonoRa 750i/ELT10000). The spectral excitation was produced by using the 488 nm argon-ion laser.

Results and Discussion

Figure 1(b) shows the X-ray diffraction (XRD) patterns of pristine Si and Si/Carbon nano-composite. All the samples show a number of XRD peaks, positioned at 28.4, 47.3 and 56.1, that can be easily indexed as cubic silicon in the Joint Committee on Powder Diffraction Standards (JCPDS) database (JCPDS No. 65-1060, space group: Fd-3m, no. 227). XRD pattern of Si/C nano-composite is almost same as that of pristine Si. Although pristine Si is prone to be oxidized by thermal energy and trapped oxygen during the heat-treatment, neither SiO_2 peaks nor the weakened intensity of Si peaks are observed even after the carbon encapsulation using DL-malic acid. The crystal size of pristine Si, calculated using the Scherrer formula, is estimated to be approximately 80 nm. Also after the carbon encapsulation process, its crystal size is maintained around 80 nm. This phenomenon was clarified by SEM analyses as shown in Figure 1(c)-(d). Pristine Si has a relatively homogeneous crystalline size of less than 200 nm on average and an immaculate surface. Even after the decomposition of DL-malic acid on its surface,

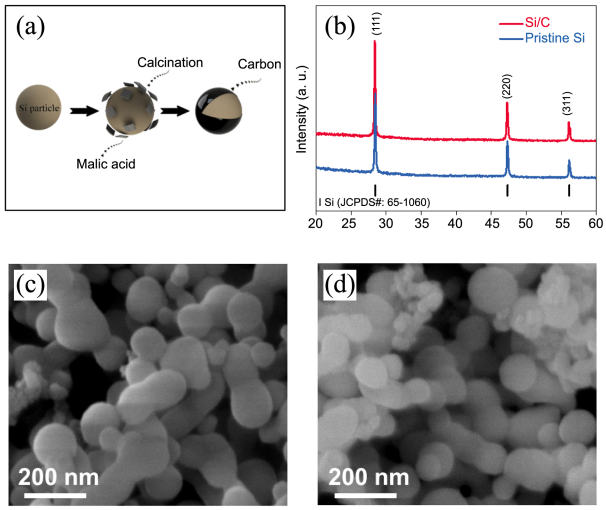

Figure 1. (a) Schematic diagram for low-temperature carbon coating process of Si/C nano-composite, structural comparison between pristine Si and Si/C nano-composite; (b) XRD patterns of Si and Si/C nano-composite, (c) SEM micrographs of pristine Si, (d) SEM micrographs of Si/C nano-composite.

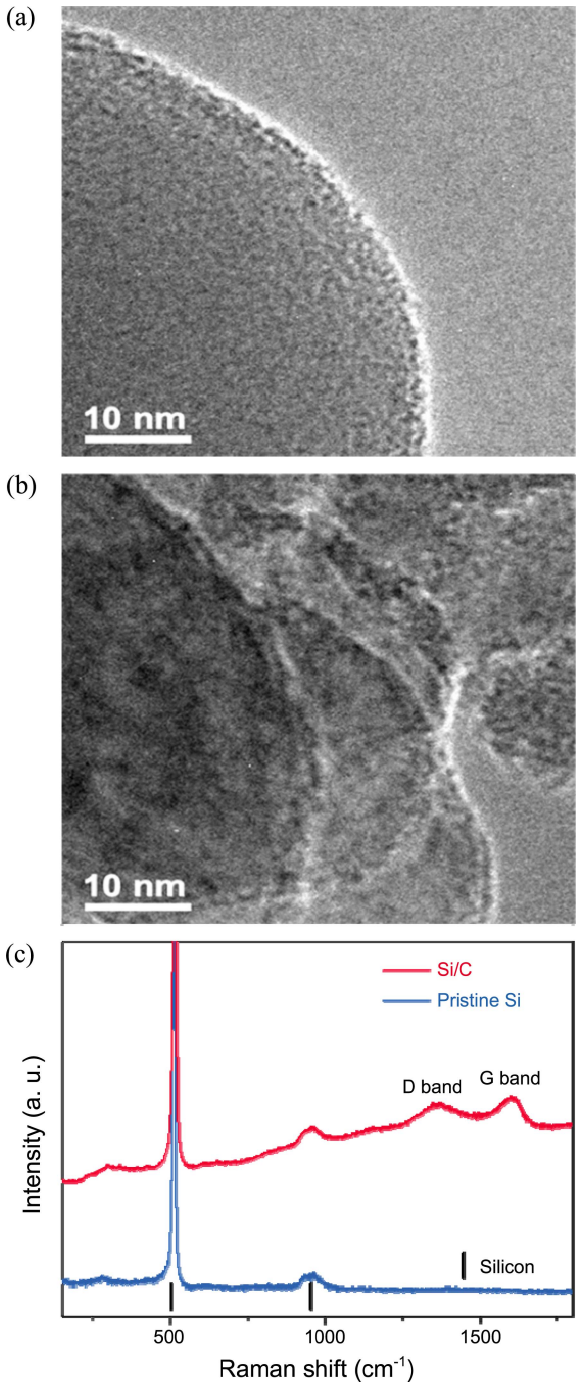

Figure 2. HRTEM images of (a) pristine Si and (b) Si/C nano-composite, (c) Raman spectra of pristine Si and Si/C nano-composite.

any morphological enlargement or agglomeration does not appear in local area indicating that there are no obvious physical changes during the carbon encapsulation process using DL-malic acid, and its process temperature is enough low not to change bulk or surface of the coated material, Si.

Figure 2 shows the HRTEM images of pristine Si and Si/C nano-composite. Herein, Si/C nano-composite clearly has a thin layer on its surface, which may be composed of amorphous carbon. The blurred image observed on the surface of Si after decomposing DL-malic acid is associated with the amorphous character of this layer (Figure 2(b)). The Raman spectra of Si/C nano-composite is apparently evident of the evolution of amorphous carbon layer on the surface of Si. Figure 2(c) compares the Raman spectra of pristine Si with that of Si/C nano-composite. In case of pristine Si, strong peaks attributed to Si-Si bond are observed, which are located at 505 cm^{-1} and 955 cm^{-1} corresponding to Si nanoparticle.[30] After the decomposition of DL-malic acid with Si nanoparticles, the broad peaks at 1345 cm^{-1} and 1602 cm^{-1} corresponding to D (Disordered) band and G (Graphitic) band evolved. These peaks are in good agreement with Raman spectra of amorphous carbon reported in various literatures.[31,32] Figure 3(a) shows the initial charge/discharge profiles of pristine Si and Si/C nano-composite between 0.005 V and 1.5 V at a current density of 0.05 C. The presence of long flat plateaus during both lithiation and delithiation indicates that Si/C nano-composite undergoes reversible two-phase transitions. During the initial lithiation, Si/C nano-composite attains very high capacity coming up to 2792 $mAhg^{-1}$, which is attributed to the formation of a high stoichiometric intermetallic compound between Li and Si, $Li_{15}Si_4$. The differential capacity plots (dQ/dV *vs.* V) of Si/C nano-composite well proves this because a lot of previous reports demonstrate that $Li_{15}Si_4$ tends to be formed below 100 mV upon reduction and decomposed around 430 mV upon oxidation in great accordance with the inset of Figure 3(a).[25,33] It has been known that $Li_{15}Si_4$ is the highest lithiated phase of Si achievable for the particular Si at the ambient temperature. Even though there is no significant evidence for side reactions including SEI (Solid Electrolyte Interphase) film formation or acidic attack in the charge/discharge profile, the enhanced initial coulombic efficiency (75%) of Si/C nano-composite compared to pristine Si (70%) implies that its amorphous carbon layer significantly contributes to stabilizing SEI film.[34,35]

Figure 3(b) presents the cyclic retentions of pristine Si and Si/C nano-composite. Si/C nano-composite clearly demonstrates its superior cyclic performance and better long-term stability in comparison with pristine Si.

At the 30th cycle, this reversible capacity decreases to nearly 840 $mAhg^{-1}$, which is still much larger than that of pristine Si. The main reason for this considerable cyclic retention seems to be associated with the amorphous carbon layer existing on the surface of Si nanoparticles. This carbon layer can thermodynamically stabilize the surface of Si nanoparticles by terminating dangling bonds of Si resultantly preventing its agglomeration upon cycling due to the reduced surface free energy. Moreover, the carbon layer that can provide facile strain relaxation well accommodates the volume expansion of Si, and ensures good electronic contact around Si as proven by the impedance analyses before or after cycling. Figure 3(c) compares the nyquist plots of pristine Si and Si/C nano-composite. The plots exhibit definitely different behaviors between pristine Si and Si/C nano-composite in the size and shape of semicircles as shown in Figure 3(c). The semicircle diameter of Si/C nano-composite (~50 $\Omega \cdot cm^2$) is much smaller than that of pristine Si (~90

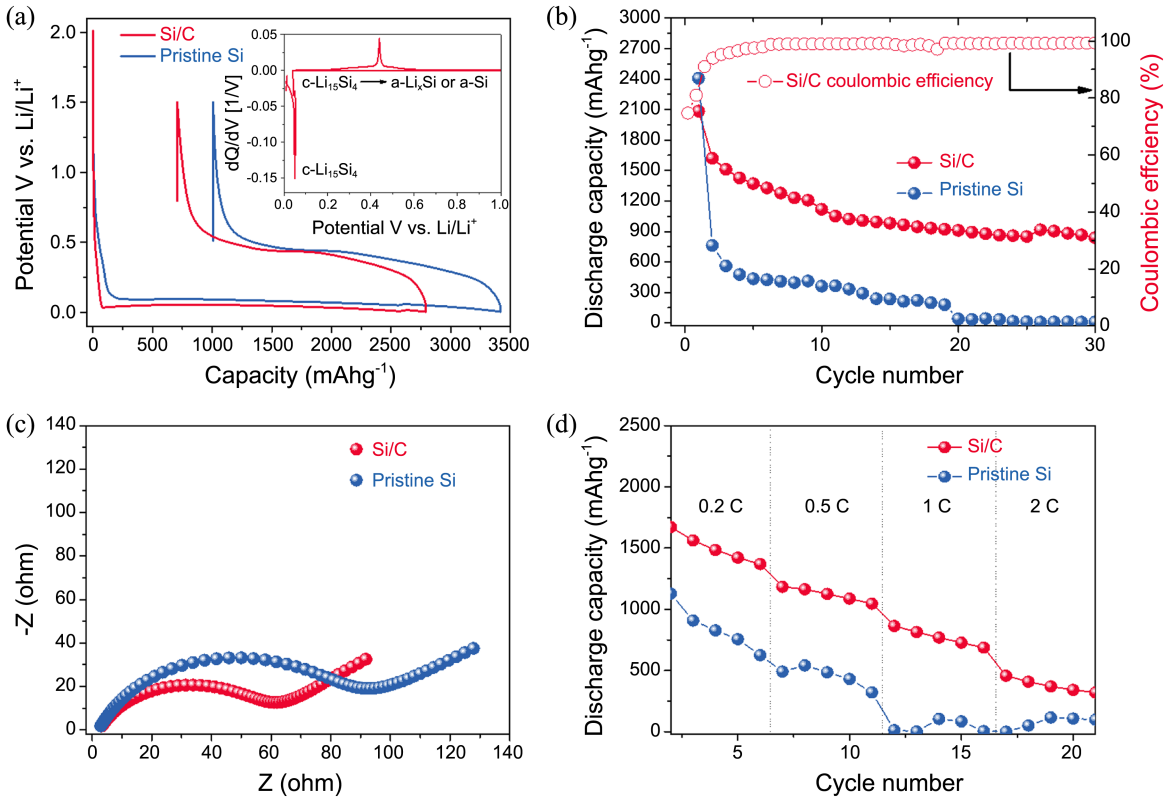

Figure 3. The electrochemical performance comparison between pristine Si and Si/C nano-composite; (a) the initial galvanostatic charge/discharge curves at 0.05 C (inset figure: the initial differential capacity plot of Si/C nano-composite), (b) cyclic performance of pristine Si and Si/C nano-composite at 0.1 C, (c) nyquist plots of pristine Si and Si/C nano-composite obtained after 1st cycle, (d) discharge capacity retention of pristine Si and Si/C nano-composite at various current rates.

$\Omega \cdot cm^2$), indicating much lower cell impedance ascribed to the existence of conductive carbon layer. Figure 3(d) shows the discharge capacity retention of pristine Si and Si/C nano-composite at different discharge current density. The rate capability is an important parameter to decide whether an electrode material can be applied to high power-density devices like electric vehicles, power tools and so forth. Even if Si-based materials have been reported to have incompetent rate capability due to its charge/discharge mechanism based on the chemical reaction between Si and Li, the discharge capacity retention of Si/C nano-composite seems to weakly depend on the discharge rate compared to pristine Si. As mentioned above, this enhanced kinetic performance of Si/C nano-composite results from the surface carbon layer leading to the increase of electrical conductivity. Even if the suggested core/shell idea was helpful to the electrochemical enhancement of Si, we think that the substitution of graphene layer for the amorphous carbon layer correlated with the replacement of Si by Si sub-oxides (SiO_x) will be one of the most probable future ways to enable Si-based materials to be commercialized in place of graphite.

Conclusion

The encapsulating carbon layer of Si/C nano-composite was successfully synthesized *via* the decomposition of DL-malic acid ($C_4H_6O_5$) at low temperature. Because this process was conducted at enough low temperature to prevent the physical change of Si, the morphology and crystalline of Si was unchanged before or after this process. Si/C nano-composite displayed high reversible capacity around 840 $mAhg^{-1}$ even after 30 cycles as well as a significantly enhanced cyclic and kinetic performance compared to pristine Si. The improved electrochemical performance of Si/C nano-composite could be attributed to a surge of electrical conductivity and an ensured surface stability provided by the existing amorphous carbon layer on the surface of Si nanoparticles. Furthermore, this layer can serve as a buffering agent to absorb the volume expansion of Si during lithiation or delithiation. Therefore, Si/C nano-composite synthesized by low-temperature decomposition of DL-malic acid would allow one to create next-generation lithium rechargeable batteries featuring significantly improved energy density.

Acknowledgments. This work was supported by the Dongguk University Research Fund of 2012.

References

1. Tarascon, J. M.; Armand, M. *Nature* **2008**, *451*, 652.
2. Maier, J. *Nature Mater.* **2005**, *4*, 805.
3. Chen, J.; Xu, L.; Li, W.; Gou, X. *Adv. Mater.* **2005**, *17*, 582.
4. Hossain, S.; Kim, Y. K.; Saleh, Y.; Loutfy, R. *J. Power Sources* **2006**, *161*, 640.
5. Winter, M.; Besenhard, J. O.; Spahr, M. E.; Novak, P. *Adv. Mater.*

1998, *10*, 725.
6. Johnson, B. A.; White, R. E. *J. Power Sources* **1998**, *70*, 48.
7. Obrovac, M. N.; Christensen, L. *Electrochem. Solid-State Lett*. **2004**, *7*, A93.
8. Niu, J. J.; Lee, J. Y. *Electrochem. Solid-State Lett*. **2002**, *5*, A107.
9. Ng, S. H.; Wang, J. Z.; Wexler, D.; Konstantinov, K.; Guo, Z. P.; Liu, H. K. *Angew. Chem. Int. Ed*. **2006**, *45*, 6896.
10. Holzapfel, M.; Buqa, H.; Scheifele, W.; Novak, P.; Petrat, F. M. *Chem. Commun*. **2005**, *12*, 1566.
11. Kang, Y. M.; Go, J. Y.; Lee, S. M.; Choi, W. U. *Electrochem. Commun*. **2007**, *9*, 1276.
12. Kang, Y. M.; Lee, S. M.; Kim, S. J.; Jeong, G. J.; Sung, M. S.; Choi, W. U.; Kim, S. S. *Electrochem. Commun*. **2007**, *9*, 959.
13. Zhang, W. M.; Hu, J. S.; Guo, Y. G.; Zheng, S. F.; Zhong, L. S.; Song, W. G.; Wan, L. J. *Adv. Mater*. **2008**, *20*, 1160.
14. Lee, Y. M.; Kang, Y. M. *J. Power Sources* **2011**, *196*, 10686.
15. Lee, Y. M.; Jo, M. R.; Song, K. S.; Nam, K. M.; Park, J. T.; Kang, Y. M. *ACS Appl. Mater. Interfaces* **2012**, *4*, 3459.
16. Ji, L.; Zhang, Y. *Energy Environ. Sci.* **2011**, *4*, 3611.
17. Chan, C. K.; Zhang, X. F.; Cui, Y. *Nano Lett*. **2008**, *8*, 307.
18. Weydanz, W. J.; Wohlfahrt, M.; Huggins, R. A. *J. Power Sources* **1999**, *81*, 237.
19. Wolfenstine, J. *J. Power Sources* **1999**, *79*, 111.
20. Peng, K.; Jie, J.; Zhang, W.; Lee, T. S. *Appl. Phys. Lett*. **2008**, *93*, 033105.
21. Park, M. H.; Kim, M. G.; Joo, J.; Kim, K.; Kim, J.; Ahn, S.; Cui, Y.; Cho, J. *Nano Lett*. **2009**, *9*, 3844.
22. Hatchard, T. D.; Dahn, J. R. *J. Electrochem. Soc*. **2004**, *151*, A838.
23. Obrovac, M. N.; Krause, L. J. *J. Electrochem. Soc*. **2007**, *154*, A103.
24. Park, M. S.; Rajendran, S.; Kang, Y. M.; Han, K. S.; Han, Y. S.; Lee, J. Y. *J. Power Sources* **2006**, *158*, 650.
25. Park, M. S.; Kang, Y. M.; Rajendran, S.; Kwon, H. S.; Lee, J. Y. *Mater. Chem. Phys*. **2006**, *496*, 100.
26. Wang, C. S.; Wu, G. T.; Zhang, X. B.; Qi, Z. F; Li, W. Z. *J. Electrochem. Soc.* **1998**, *145*, 2751.
27. Wilson, A. M.; Dahn, J. R. *J. Electrochem. Soc.* **1995**, *142*, 326.
28. Hu, Y. S.; Demir-Cakan, R.; Titirici, M. M.; Müller, J. O.; Schlögl, R.; Antonietti, M.; Maier, J. *Angew. Chem. Angew. Chem. Int. Ed*. **2008**, *120*, 1669.
29. Park, M. S.; Wang, G. X.; Kang, Y. M.; Wexler, D.; Dou, S. X.; Liu, H. K. *Chem. Angew. Chem. Int. Ed*. **2007**, *46*, 750.
30. Meiera, C.; Luttjohanna, S.; Kravetsa, V. G.; Nienhausa, H.; Lorkea, A.; Wiggersb, Hartmut. *Physica E* **2006**, *32*, 155.
31. Pasteris, J. D.; Wopenka, B. *Astrobiology* **2003**, *3*, 727.
32. Yang, C. J.; Jiang, J. L.; Ping, D. J.; Fei, Z. H. *Chin. Phys. Lett*. **2008**, *25*, 780.
33. Kang, K.; Lee, H.; Han, D.; Kim, G.; Lee, D.; Lee, G.; Kang, Y. M.; Jo, M. *Appl. Phys. Lett.* **2010**, *96*, 053110.
34. Park, M. S.; Kang, Y. M.; Kim, J. H.; Wang, G. X.; Dou, S. X.; Liu, H. K. *Carbon* **2008**, *46*, 35.
35. Hassan, M. F.; Guo, Z. P.; Chen, Z.; Liu, H. K. *J. Power Sources* **2010**, *195*, 2372.